The weak shear phase diagram for nematic polymers *

M. G. Forest †, Qi Wang ‡, and R. Zhou §

May 8, 2002

Abstract

We study the weak shear problem of nematic polymers as modeled by the kinetic theory of Doi [4] and Hess [15]. The probability distribution function (pdf) $f(\mathbf{m}, t)$ is to be solved for the orientation of rigid molecules with axis of symmetry $\mathbf{m} \in S^2$ (the sphere) due to the interaction of an excluded-volume potential (with strength proportional to dimensionless concentration N) and an imposed shear flow with normalized shear rate Pe. Quiescent nematic liquids are characterized by their degree of order versus nematic concentration (the classical isotropic-nematic phase diagram), wherein f is *orientationally degenerate* [10]: each stationary distribution except the isotropic state, and every transient solution for arbitrary initial data, generates an orthogonal group $O(3)$ of solutions $f(\mathbf{U}\mathbf{m}, t)$, for any $U \in O(3)$. At the onset of weak shear, $0 < Pe \ll 1$, this degeneracy (symmetry) is broken, and monodomain selection criteria are notoriously difficult: How many stationary distributions f survive? Which are stable? Are they steady or unsteady? How do these properties vary with concentration N? Faraoni et al. and Maffettone et al. [6, 14] have used numerical bifurcation software (AUTO) together with spherical harmonic expansions to determine monodomain attractors and transition curves for significant regions of the parameter space (N, Pe). We complement their studies by a combined mesoscopic-microscopic strategy to resolve subtle aspects of the weak shear phase diagram. Analysis and numerical results from moment-closure models [9, 11] are used as a predictor. We then employ kinetic simulations to confirm the robust features of mesoscopic predictions, and to resolve and remove sensitivity associated with closure approximations.

*UNC-CH Program in Applied Mathematics Preprint Series No. PAMPS-2002-16
†Department of Mathematics, University of North Carolina at Chapel Hill, Chapel Hill, NC 27599-3250
‡Mathematics, Florida State University, Tallahassee, FL 32306
§Department of Mathematics, University of North Carolina at Chapel Hill, Chapel Hill, NC 27599-3250

1 The Doi kinetic theory

We recall the basic elements of the Doi kinetic theory for nematic polymers in simple shear flows. In order to make explicit contact with the results of Faraoni et. al. [6] and Grosso et. al. [14], we restrict to infinite-aspect-ratio rigid rods. Let $f(\mathbf{m},t)$ be the *orientational probability distribution function* (pdf) for molecules with axis of symmetry $\mathbf{m}$ on the unit sphere S^2. The Smoluchowski (kinetic) equation for $f(\mathbf{m},t)$ in an imposed shear flow field $\mathbf{v}$ is given by [4, 15]:

$$\begin{aligned} &\tfrac{Df}{Dt} = \mathcal{R}\cdot[D_r(\mathbf{m})(\mathcal{R}f + \tfrac{1}{kT}f\mathcal{R}V)] - \mathcal{R}\cdot[\mathbf{m}\times\dot{\mathbf{m}}f], \\ &\dot{\mathbf{m}} = \mathbf{\Omega}\cdot\mathbf{m} + [\mathbf{D}\cdot\mathbf{m} - \mathbf{D}:\mathbf{mmm}], \end{aligned} \tag{1}$$

where $D_r(\mathbf{m})$ is the rotary diffusivity which we hold constant, $D_r(\mathbf{m}) = D_r^0$, again to make contact with [6, 14]; k is the Boltzmann constant; T is absolute temperature; $\mathcal{R} = \mathbf{m}\times\frac{\partial}{\partial\mathbf{m}}$ is the rotational gradient operator; and $\frac{D}{Dt}(\bullet)$ denotes the material derivative $\frac{\partial}{\partial t}(\cdot) + \mathbf{v}\cdot\nabla(\cdot)$, $\mathbf{v}$ is given in Cartesian coordinates (x,y,z) with shear rate $\dot\gamma$ by

$$\mathbf{v} = \dot\gamma(y,0,0)\,, \tag{2}$$

from which $\mathbf{D}$ and $\mathbf{\Omega}$ are the corresponding rate-of-strain and vorticity tensors,

$$\mathbf{D} = \frac{1}{2}\dot\gamma\begin{pmatrix} 0 & 1 & 0 \\ 1 & 0 & 0 \\ 0 & 0 & 0 \end{pmatrix}, \mathbf{\Omega} = \frac{1}{2}\dot\gamma\begin{pmatrix} 0 & 1 & 0 \\ -1 & 0 & 0 \\ 0 & 0 & 0 \end{pmatrix}. \tag{3}$$

The Peclet number is $Pe = \dot\gamma/Dr^0$. For this paper, we limit $0 \le Pe \le 1$. In (1), the second-moment of the pdf f,

$$\mathbf{M} = \langle\mathbf{mm}\rangle = \int_{||\mathbf{m}||=1} \mathbf{mm}\, f(\mathbf{m},t)\, d\mathbf{m}. \tag{4}$$

enters through the mean-field, Maier-Saupe excluded-volume potential V,

$$V = -\frac{3}{2}N\,kT\,\mathbf{mm}:\mathbf{M}\,, \tag{5}$$

where N is the dimensionless strength of the potential V, proportional to the concentration of rods and inversely proportional to temperature. The *mesoscopic orientation tensor* $\mathbf{Q}$ is the traceless part of $\mathbf{M}$,

$$\mathbf{Q} = \mathbf{M} - \tfrac{1}{3}\mathbf{I}\,, \tag{6}$$

whose entries are measurable in the laboratory, e.g., see [12, 1].

2 Spherical harmonic expansion and second-moment projection of f

Let θ, ϕ be spherical coordinates with θ the polar angle measured from the vorticity axis (z) and ϕ the latitude angle in the shear plane (x, y), measured counter-clockwise from the positive flow direction (x); y is the flow-gradient direction. The molecule axis $\mathbf{m} \in S^2$ is then represented by

$$\mathbf{m} = (\sin\theta\, \cos\phi, \sin\theta\, \sin\phi, \cos\theta)\,. \tag{7}$$

As in [20, 6, 14], we seek solutions of (1)-(6) in the form of a spherical harmonic expansion,

$$f(\mathbf{m}, t) = \sum_{l=0}^{L} \sum_{m=-l}^{l} a_{l,m}(t) Y_l^m(\theta, \phi), \tag{8}$$

where Y_l^m are complex spherical harmonic functions [26],

$$Y_l^m = P_l^m(\cos\theta) e^{im\phi}, \tag{9}$$

P_l^m are Legendre polynomials, and L is the order of truncation in the Galerkin approximation. The projection of f onto its traceless second moment $\mathbf{Q}$ is explicitly given by

$$\begin{aligned}
Q_{xx} &= -\tfrac{2}{3}\sqrt{\tfrac{\pi}{5}}\, a_{2,0} + \sqrt{\tfrac{8\pi}{15}}\Re(a_{2,2}) \\
Q_{yy} &= -\tfrac{2}{3}\sqrt{\tfrac{\pi}{5}}\, a_{2,0} - \sqrt{\tfrac{8\pi}{15}}\Re(a_{2,2}) \\
Q_{xy} &= \sqrt{\tfrac{8\pi}{15}}\Im(a_{2,2}) \\
Q_{xz} &= -\sqrt{\tfrac{8\pi}{15}}\Re(a_{2,1}) \\
Q_{yz} &= -\sqrt{\tfrac{8\pi}{15}}\Im(a_{2,1})\,,
\end{aligned} \tag{10}$$

where, $\Re(\cdot)$ and $\Im(\cdot)$ represent real and imaginary parts, respectively. In simulations below, we follow tradition and project $f(\mathbf{m}, t)$ onto its second moment, $\mathbf{Q}(f(\mathbf{m}, t))$ or $\mathbf{M}(f(\mathbf{m}, t))$. The eigenvalues of $\mathbf{M}$ are ordered $0 \le d_3 \le d_2 \le d_1 \le 1$ ($\mathbf{Q}$ has eigenvalues $d_i - \frac{1}{3}$); $\mathbf{Q}$ and $\mathbf{M}$ share a basis of orthogonal eigenvectors $\mathbf{n_1}, \mathbf{n_2}, \mathbf{n_3}$. This defines the *major director* for $f(\mathbf{m}, t)$, given by the direction $\mathbf{n}_1$ of maximum degree d_1 of mesoscopic alignment.

3 The weak shear problem

Figure 1 depicts the equilibrium ($\mathbf{v} = \mathbf{0}$) isotropic-nematic phase diagram [3, 6, 14]. This standard representation of the isotropic ($d_i = \frac{1}{3}, i = 1, 2, 3$) and nematic equilibria f_* of

(1) arises by projection of f_* onto the second-moment $\mathbf{Q}(f_*)$, (10), which are all uniaxial ($d_i = d_j$ for at least two $i \neq j$) for the Maier-Saupe potential [3]. Thus $\mathbf{Q}(f_*)$ is specified by the simple eigenvalue of $\mathbf{Q}(f_*)$, plotted in Figure 1 to yield the traditional isotropic-nematic (I-N) phase diagram, repeated from [10] and in agreement with [6]. By design [3], this picture removes the underlying $O(3)$ symmetry of the Smoluchowski equation (1) with $\mathbf{v} = 0$. *The nematic solution branches, $s_\pm$, correspond to an entire $O(3)$ group of equilibria, and the saddle-node bifurcation at $N \approx 4.49$ is an $O(3)$ of saddle-nodes.* Furthermore, all initial-value solutions for arbitrary anisotropic initial data $f(\mathbf{m}, 0) \neq \frac{1}{4\pi}$ are $O(3)$ degenerate, i.e., each orbit $f(\mathbf{m}, t)$ generates an entire continuous group of orbits $f(\mathbf{U}\mathbf{m}, t)$ for all $\mathbf{U} \in O(3)$ [10]. The $O(3)$ symmetry projects onto the second-moment tensor in the form $\mathbf{U}^T\mathbf{Q}\mathbf{U}$ [9].

This underlying symmetry is broken by any generic perturbation. In the case of weak flows such as shear, the selection mechanisms that determine which stationary orientational distributions persist, either as steady or unsteady states, have remained elusive. Early seminal work is due to Hess, Semenov, Kuzuu, Doi, Marrucci, Greco, and Maffettone [15, 28, 29, 17, 18, 25, 22, 23, 24] which aim to construct stationary distribution functions. To foreshadow our approach, we note that *saddle-node bifurcations are structurally stable*, so SN_0 of Figure 1 will survive in weak shear. The $O(3)$ symmetry of f, inherited by $\mathbf{Q}$, is responsible for the continuous multiplicity of SN_0. Since this full symmetry will not survive shear flow perturbations, the *discrete, finite multiplicity of SN bifurcations is a primary structure* to be determined. By contrast, the transcritical bifurcation TC_0 of Figure 1 is structurally unstable, and will be destroyed by generic perturbations. The fate of TC_0 in weak shear, because of the associated non-degeneracy of the isotropic state s_0, is far easier to determine. After controlling the discrete bifurcations surviving from SN_0 and TC_0, we track yet more difficult issues of steady-unsteady transitions, in-plane to out-of-plane transitions, and the stability of all branches of solutions.

Significant understanding of the shear problem for nematic polymers has come from numerical simulations of kinetic theory, beginning with Larson and Ottinger [19, 20] and continuing over the past decade. The most complete results, covering large regions of the (N, Pe) parameter space, are given by Faraoni et al. and Grosso et al. [6, 14]; our purpose here is to further elucidate the *selection mechanisms in the weak shear limit*, and to progress further toward a rigorous theory of the number and type of stationary kinetic theory distributions that survive in weak shear flow across the nematic concentration range that encompasses the I-N transition. Once the shear-onset problem is solved, the continuation problem to finite shear rates is tractable from numerical continuation software, although we shall reveal infinite-period bifurcations beyond current numerical resolution and in need of theoretical guidance. Rigorous kinetic bifurcation theory remains an outstanding challege.

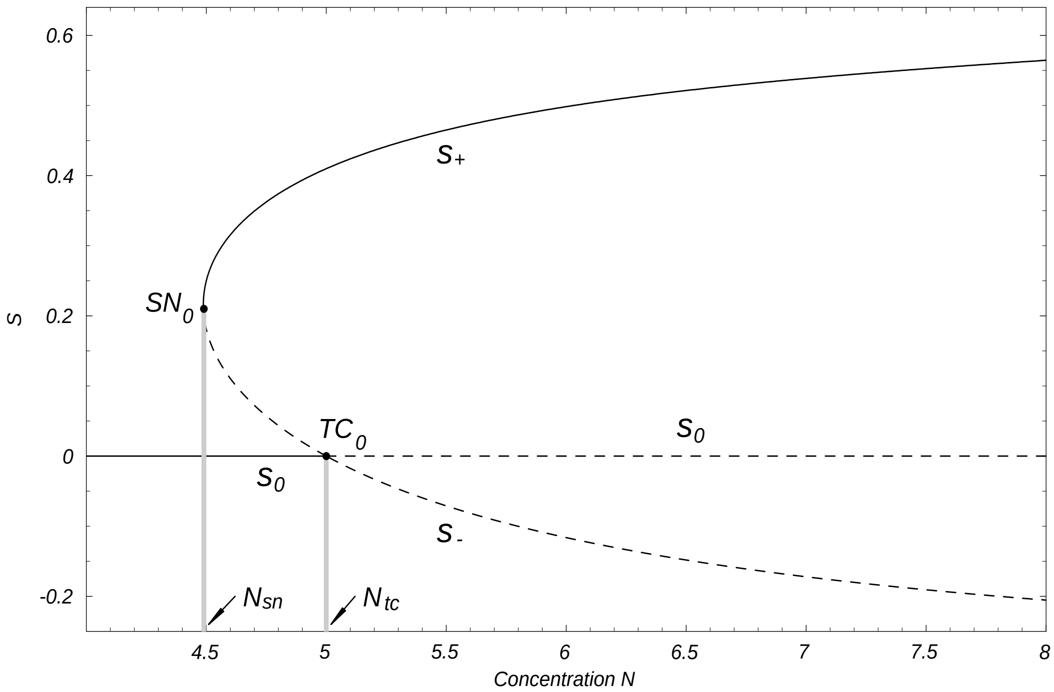

Figure 1: **The isotropic-to-nematic phase diagram for quiescent nematic liquids of infinite aspect ratio**, from [10]. The curves depict equilibria f_* of the Smoluchowski equation (1) without flow ($\mathbf{v} = \mathbf{0}$), versus nematic concentration, N. The vertical axis depicts the uniaxial order parameter, s_*, derived from the projection of f_* onto the second-moment tensor $\mathbf{Q}_*$, from which s_* is the simple eigenvalue. Solid lines represent stable, dashed lines unstable, steady solutions. $f_0 = \frac{1}{4\pi}$ is the isotropic state which exists for all N, whose second-moment tensor $\mathbf{Q}_0 = \mathbf{0}$ and $s_0 = 0$; the isotropic equilibrium is isolated, and non-degenerate. The nematic branches $f_\pm$ correspond to an entire $O(3)$ of equilibria of the form $f_\pm(\mathbf{Um})$ for all $\mathbf{U} \in O(3)$. The projections of $f_\pm$ onto second-moment tensors, $\mathbf{Q}_\pm$, share this symmetry, $\mathbf{U}^T\mathbf{Q}_\pm\mathbf{U}$. The order parameter projections are unique, and hide the orientational degeneracy of the nematic equilibria in which the orthonormal frame of directors of $\mathbf{Q}$ lies arbitrarily on the sphere.

We substitute the spherical harmonic expansion (8) into the Smoluchowski equation (1) and project the equation onto the subspace spanned by $G = Y_l^m, m = -l, \cdots, l, l = 0, \cdots, L$. This yields a $[L(L+3)/2]$-dimensional system of ordinary differential equations for $a_{l,m}(t), m = -l, \cdots, l, l = 0, \cdots, L$. Our numerical studies show robust results if $L = 10$, which we check in random parameter regimes with larger L. In the highly concentrated regime, $N > 8$, a significantly higher order truncation is required to resolve the small-scale structure of f.

We refer to [10] for details about the form of the ode system for $a_{l,m}(t)$, and symmetry properties of (1)-(6) with imposed shear. We recall relevant results:

- The Smoluchowski equation (1)-(6) admits an *invariant subspace of in-plane orientation distributions* f, $a_{l,m} = 0$ for all m odd, which generalizes the in-plane mesoscopic tensor criterion $Q_{xz} = Q_{yz} = 0$.

This fact is exploited here to detect out-of-plane solutions and to detect out-of-plane instabilities of in-plane stable solutions. (Both features are immediate from a comparison of Figures 2 and 3.)

- All *out-of-plane solutions* f of (1)-(6) have major director which *remains out-of-plane*, and cannot reach the shearing plane except in infinite time. Each such out-of-plane orbit f has a *mirror-symmetric orbit* $\hat{f}$ whose major director is tilted to the other side of the shearing plane.

f and $\hat{f}$ are explicitly related by the transformation $\hat{a}_{l,m} = (-1)^m a_{l,m}$, which affords a strong benchmark on the numerical bifurcation software. Many out-of-plane solution pairs are determined below; when stable, they automatically instill *bistability.* Explicit examples include the out-of-plane steady states labelled **OS**, and periodic solutions we call "tilted kayaking" or "out-of-plane wagging" labelled $\mathbf{K}_2$, which were identified in kinetic simulations by Faraoni et al. [6], who further recognized their mirror-symmetry. These $\mathbf{K}_2$ orbits have major director which oscillates around an axis that lies strictly between the vorticity axis and shear plane.

- The logrolling steady states (**LR**) and classical kayaking orbits ($\mathbf{K}_1$) of Larson and Ottinger, whose major director aligns with and rotates around the vorticity axis, respectively, are mapped to themself under reflection through the shear plane. Along with all in-plane distributions, **LR** and $\mathbf{K}_1$ solutions arise in single isolated branches.

These kinetic theory symmetries assert global constraints on the space of solutions for (1)-(6). We progress now to a finer resolution of the attractors and unstable states that survive in weak shear, and the relationship between kinetic theory and tensor approximations. Mesoscopic analysis and simulations [9, 11] *predict* explicit counts of the multiplicity and stability of monodomain solution branches versus nematic concentration N and normalized shear rate Pe, for Doi-type tensor models; similar methods [27, 21] infer in-plane transitions versus shear rate for Hess-type tensor models. These methods apply to any tensor model and allow one to delineate shear-selection criteria that are robust versus sensitive to closure approximation, and to determine model-specific phase transitions as one varies molecular aspect ratio, nematic concentration, or shear rate. As we detail next, the "mesoscopic predictor" is followed by kinetic theory simulations guided by the above symmetry properties, from which we confirm the robust features and "correct" the sensitive features. This predictor-corrector perspective of mesoscopic simulations has been advocated by Kevrekidis et al. [30, 13].

The overwhelming wealth of intuition about the shear problem for nematic polymers has derived from continuum theory of Leslie and Erickson and mesoscopic tensor theory of Landau-deGennes, Hess, Doi-Edwards, Beris-Edwards-Grmela. (we refer to [9] for an extensive literature discussion.) In [9, 11] mesoscopic analysis identifies parameter regimes for either of eight distinct tensor models where a precise count of the number of solutions which break the continuous $O(3)$ degeneracy can be given, and the stability of all solution branches is determined. It is now recognized that mesoscopic tensor models are recoverable from closure approximations of either Hess [15] or Doi [4] kinetic theory; recent illustrations are given in [27, 21, 9]. Abundant evidence shows the selection mechanisms in weak shear are highly sensitive to closure. We maintain that the prudent approach to resolve this model sensitivity is by appeal to the microscopic kinetic theory of Doi and Hess. Because of the orientational degeneracy inherent in the mean-field intermolecular potential, the truncation of the infinite-dimensional Smoluchowski equation (1) onto a five-dimensional, mesoscopic tensor dynamical system is too crude of an approximation across the range of nematic concentrations that encompass the quiescent isotropic-nematic transition and the onset of weak shear. Indeed, one finds that orders of magnitude greater resolution in the spherical harmonic expansions of f are required to get robust numerical simulations [6, 14, 10], and thereby remove ambiguities due to the projection onto second-moment tensor systems. It is nonetheless remarkable that specific kinetic theory features associated with restricted regions of parameter space are qualitatively preserved by individual tensor models; the period-doubling route to chaotic dynamics [14] captured by the Doi closure [9] is one notable example. Various features shared (or not) by kinetic theory and closure approximations are reported below.

4 Kinetic theory results

In [9, 11], mesoscopic models determine the following *robust features that are confirmed from the Smoluchowski kinetic simulations in Figures 2,3.* As in Figure 1, we label critical concentrations N_* at which phase transitions (bifurcations) occur, with $_*$ chosen consistent with the bifurcation type and number, e.g., N_{sn_-} for the specific saddle-node SN_-. We will build up the weak-shear-perturbed pictures by first ascertaining *the fate of the saddle-node* (SN_0) *and transcritical* (TC_0) *bifurcations of quiescent nematics in Figure 1.* These features will provide the skeleton upon which we then build up the subsequent finer details.

- All stationary distributions f are steady at the onset of shear ($0 < Pe \ll 1$) if the nematic concentration N is sufficiently close to the quiescent I-N transition interval $(N_{sn}, N_{tc}) = (4.49, 5)$ of Figure 1.
- This defines a weak-shear "window" (framed in grey in Figure 2) of concentrations N for each fixed shear rate, $0 < Pe \ll 1$, $O(Pe)$ close to the quiescent I-N bifurcation window, inside of which *the* $O(3)$*-degenerate saddle-node* (SN_0) *of Figure 1 for* $Pe = 0$ *persists as* 3 *discrete* $SN_{1,2,3}$ *bifurcations*! This numerical result confirms rigorous mesoscopic analysis [11].
- In Figures 2,3, this "window" is chosen $4.40 < N < 4.60$, which encloses *the* 3 *saddle-nodes* $SN_{1,2,3}$, *another saddle node* SN_- *which detaches from the* TC_0 *bifurcation, and exactly* 7 *(seven) branches of weak-shear-selected stationary distributions* f emerging from these four SN's. We amplify this structure first.
  - The lowest-norm stable branch for $0 < N < N_{sn_-}$ in Figure 2a is the unique stationary distribution of (1) for $0 < N < N_{sn_1}$, arising from the isotropic branch s_0 of Figure 1. Mesoscopic analysis [11] predicts, and the kinetic simulation in Figure 2 confirms: this branch is *in-plane, flow-aligning (***FA***), and stable* until $N = N_{sn_-} \approx 4.48$ when it connects to the saddle-node SN_-. Far to the right ($N \geq N_{sn_+} \approx 5.64$), the dashed low-norm unstable branch in Figure 2a is also the continuation of the non-degenerate, unstable isotropic branch of Figure 1.
  - We further depict a_{20} in Figure 2 b, which by (10) is proportional to the in-plane scalar tensor quantity $Q_{xx} + Q_{yy}$.
  - The structurally unstable transcritical bifurcation TC_0 of Figure 1 "pulls apart" in weak shear, creating two opposing saddle-nodes, SN_- and SN_+ in Figure 2, 3.
  - The isotropic branch s_0 of Figure 1 remains isolated and unique, yet fails to persist for $0 < Pe \ll 1$ and concentrations between SN_- and SN_+.

Detailed properties of this stable **FA** branch for $0 < N < N_{sn_-}$ are given in Figure 4. The order-parameter projection of f indicates rather strong biaxiality, even though the degrees of orientation are weak. (All other stable flow-aligned branches at $Pe = 0.1$ are also depicted, and discussed below.) Figure 5 shows the in-plane Leslie-alignment

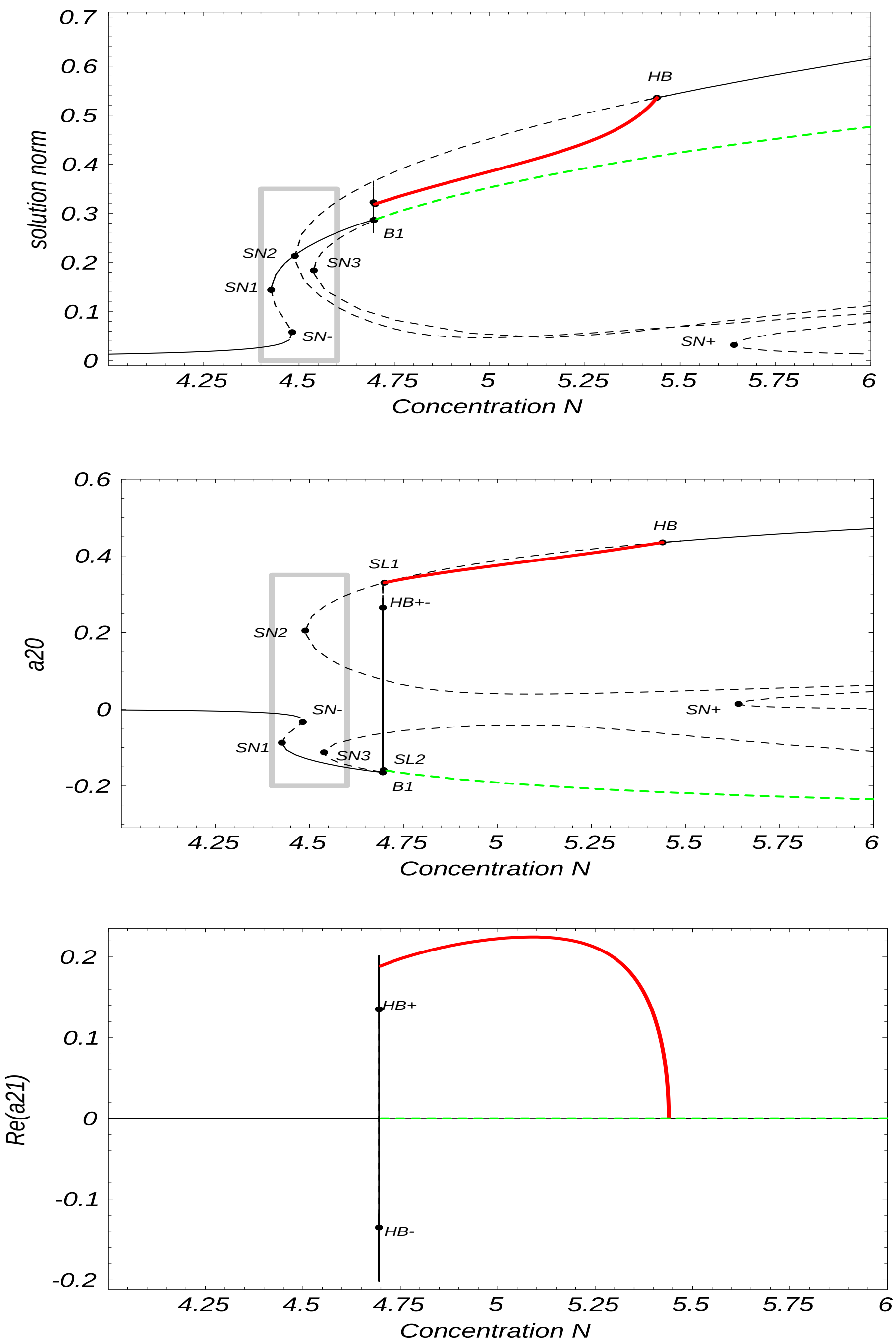

Figure 2: The bifurcation diagram of all stable and unstable orientational distribution functions f for variable concentration N and fixed weak shear $Pe = 0.1$. Solid black lines correspond to stable steady solutions described in detail in the text; dashed black lines are unstable steady solutions; the solid grey line represents stable periodic, out-of-plane kayaking solutions; and the dashed grey line corresponds to unstable periodic, in-plane tumbling and wagging solutions.

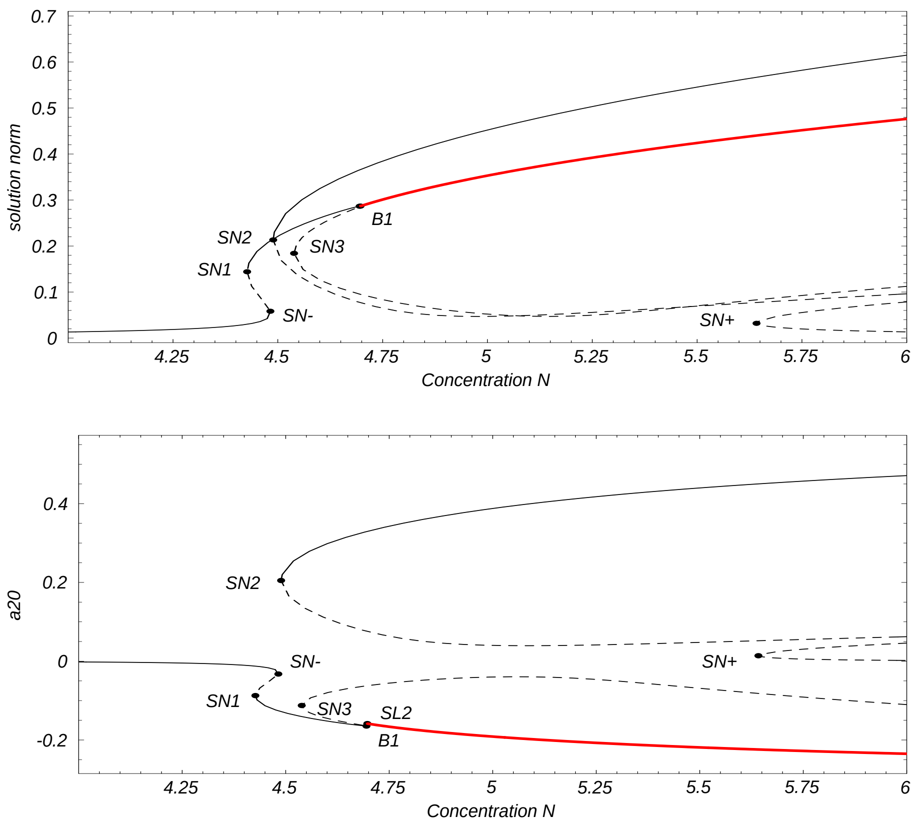

Figure 3: *In-plane bifurcation diagram* of all stable and unstable orientational distribution functions f for variable concentration N and fixed weak shear $Pe = 0.1$. Solid lines correspond to stable steady solutions, dashed lines are unstable steady solutions; the solid grey line represents stable periodic tumbling and wagging solutions. Comparison with the diagram of Figure 2 shows which in-plane distributions are stable in the restricted subspace yet unstable to out-of-plane perturbations.

angle computed by projecting f for each N onto the second-moment, then extracting the major director (which is in-plane).

- The other branch emanating from SN_- (and SN_+) in Figure 2a, 2b corresponds to one *flow-aligned, unstable state that survives from the continuous* $O(3)$ *group* s_- *of unstable equilibria from Figure 1. The branch that emerges from* SN_- *turns back for* $N < N_{sn_-}$ (and a similar branch turns ahead for $N > N_{sn_+}$ out of SN_+).

One branch connects SN_- to SN_1 in Figure 2a,2b, inside the "window" of N; the other branch continues for $N > N_{sn_+}$. Both branches are necessarily unstable at least locally for $0 < Pe \ll 1$ and for N nearby the $SN_\pm$ bifurcations by continuity of linearized eigenvalues with respect to Pe. These branches therefore inherit the instability of s_- as well as possible additional instabilities arising from breaking the two zero eigenvalues associated with orientational degeneracy.

This accounts for 4 steady branches that emerge from the TC_0 bifurcation of the quiescent I-N diagram of Figure 1, 2; two branches (O-SN_-, SN_--SN_1) lie inside the "window" defined above, the other two (dotted curves connected to SN_+) lie outside the "window". All four of these branches are *flow-aligning*, and since they emerge from the TC_0 bifurcation of Figure 1, they are nearly isotropic. Only the solid lower branch of Figure 2a for $0 < N < N_{sn_-}$ is stable. Figure 4 measures the degree of anisotropic order in this and other steady stable branches.

– In Figure 2a, 2b, *the three distinguished saddle-nodes $SN_{1,2,3}$ are the only SN's that survive from the entire $O(3)$ group of quiescent SN_0 bifurcations of Figure 1.*

Two are flow-aligning (SN_1, SN_3) orientational distributions, whereas SN_2 corresponds to a logrolling distribution; the 2 branches emerging from each of $SN_{1,2,3}$ are also in-plane or logrolling. (Otherwise they would have to undergo an instability transition to tip out-of-plane, which does not occur!) This detailed structure of multiplicity and of in-plane and vorticity alignment, can be proven rigorously for algebraic closures in the weak shear limit [11].

By continuity of linearization, once we determine the *multiplicity* 3 *of SN's surviving the quiescent saddle-node* SN_0, we know that *locally* for $N > N_{sn_j}$, $j = 1, 2, 3$, there are two branches coming out of each saddle-node, one corresponding to s_+ (the higher norm branch), the other to s_-. Equivalently, a total of 6 (six) branches of stationary equilibria are shear-selected nearby the 3 saddle-nodes $SN_{1,2,3}$, four of them are flow-aligned, and two are logrolling.

– From each $SN_{1,2,3}$, only one branch can be stable since the other necessarily has at least a 1-dimensional instability.

In Figure 2, 3, only the 3 "upper" branches associated with s_+, emanating from $SN_{1,2,3}$, are possibly stable. The delicate question is which of these 3 orientational distributions is stabilized?

Recall from [9], the multiplicity analysis is robust to closure, and from [11], for algebraic closures 3 saddle-nodes persist and they must all be "in-plane" (flow-aligning or logrolling). However, *stability of* **FA** *versus* **LR** *solution branches is closure-sensitive.* Our kinetic simulations determine:

– *for N close to the shear-selected saddle-nodes $SN_{1,2,3}$, the kinetic theory stabilizes a unique* **FA** *branch*, shown as the solid branch in Figure 2a,2b connecting SN_1 and B_1. As shown in Figure 5, this leads to a narrow band of concentrations,

$N_{sn_1} < N < N_{sn_-}$, with *bi-stable FA branches*; this represents preservation of the bi-stable concentration range of quiescent nematics, $N_{sn} < N < N_{tc}$, Figure 1.

We further depict in Figure 2 c the out-of-plane component, $Re(a_{21})$, which by (10) is proportional to Q_{xz}, whose non-zero values highlight *out-of-plane* solution branches. This graph conveys by comparison with Figures 2a, 2b that

- all 6 solution branches emerging from $SN_{1,2,3}$ are in-plane, i.e., *the major director of* $\mathbf{Q}(f)$ *is either aligned in the shearing plane or along the vorticity axis*, confirming mesoscopic rigorous results with the Doi closure model [11].

Comparison of the full Smoluchowski bifurcation diagram of Figure 2 for $Pe = 0.1$ with that of Figure 3 for the *in-plane subspace of distributions* f shows

- *the* **LR** *branch emerging from* SN_2 *is unstable specifically to out-of-plane instabilities.* Any in-plane analysis will be blind to this instability. This *director-tipping instability of the* **LR** *branch is concentration* (N)*-dependent* : the instability vanishes at higher concentrations beginning at the Hopf bifurcation labelled *HB*, so that a stable **LR** branch emerges for $N > N_{hb}$.

From [9], the low-concentration logrolling instability is captured by both the Doi and Rey-Tsuji [31] closure models, but these closures fail to capture the stabilization at higher N, i.e., they do not capture the bifurcation *HB*. The Hinch-Leal [16] closures, on the other hand, incorrectly predict stabilization of the **LR** branch nearby SN_2, fail to predict the stable **FA** branch nearby SN_1, yet correctly predict stable **LR** states at higher N.

As we move outside the "window" of Figure 2a,2b, away from the saddle-nodes $SN_{1,2,3,-}$, the three branches associated with s_+ undergo important transitions at bifurcations labelled B_1, $HB_{\pm}$,$SL_{1,2}$ (and *HB* at higher N). We amplify these phenomena next:

- B_1 is the *flow-aligning to tumbling transition*, marking entry into a band of concentrations (N_{b_1}, N_{hb}) where no stable steady distributions exist. This branch of solutions is stable in the in-plane space of distributions as shown in Figure 3, but *unstable to out-of-plane perturbations* by comparison with Figure 2.
- There is a tumbling-wagging transition on the branch in Figure 2,3 past the bifurcation B_1, but the entire branch is unstable. Only at higher values of Pe does the wagging branch stabilize through a period-doubling bifurcation (see Tables 1, 2).
- Thus *no stable tumbling or wagging states exist, and no stable steady states exist, for the concentration band* (N_{b_1}, N_{hb}) *at* $Pe = 0.1$. Note the in-plane Smoluchowski equation,

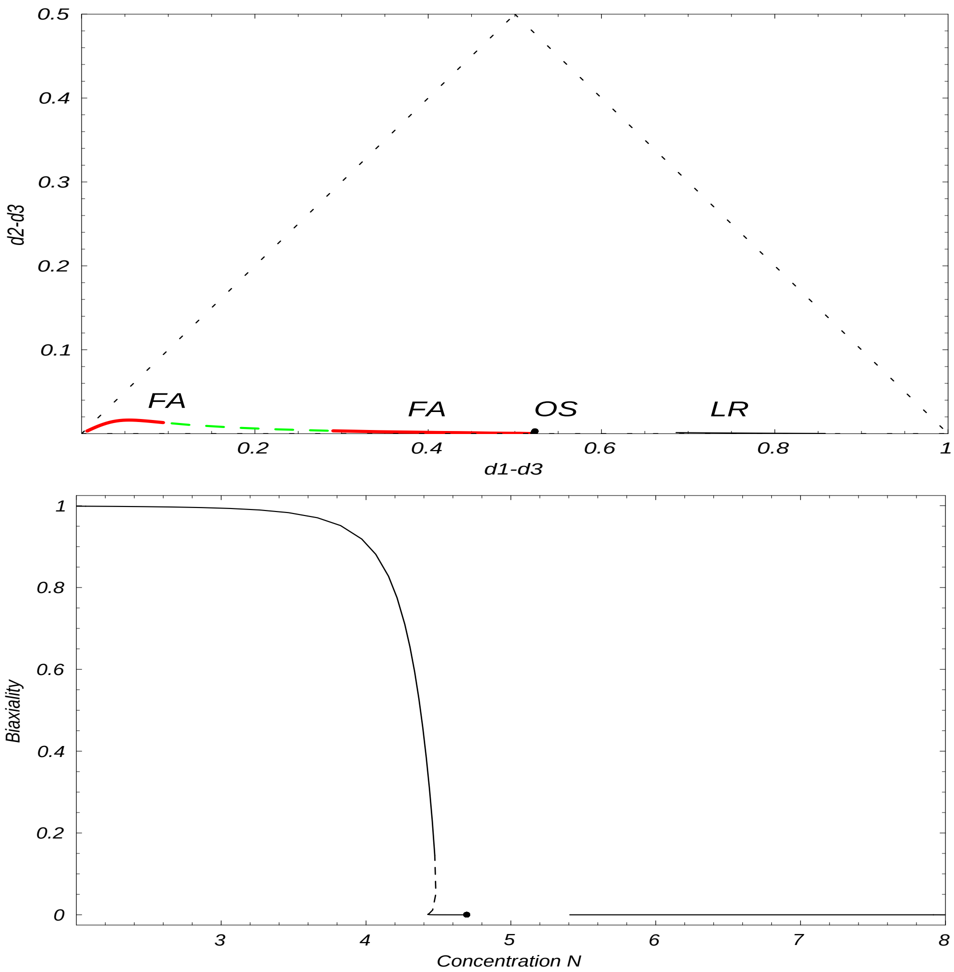

Figure 4: Order parameter projections and measures of biaxiality for all *stable steady* solution branches of Figure 2 for $Pe = 0.1$ and variable concentration N. Top: From $\mathbf{Q}(f)$, the order parameter differences $(d_1 - d_3, d_2 - d_3)$ for stable (solid) and unstable (dashed) solutions capture anisotropic order in the respective planes, $(\mathbf{n}_1, \mathbf{n}_2)$ of maximum birefringence and $(\mathbf{n}_2, \mathbf{n}_3)$ orthogonal to the major director $\mathbf{n}_1$. The lower-left corner corresponds to the flow-aligning stable branch O-SN_- that emerges from the isotropic solution $(d_1 = d_2 = d_3)$. The **OS** branch is resolved as a large dot that interpolates the **FA** and unstable logrolling branch of Figure 2. The middle stable flow-aligning branch SN_1-B_1 emerges from the stable nematic branch of Figure 2. Stable logrolling solutions **LR** also emerge from the stable nematic branch of Figure 2, with higher maximum birefringence than the **FA** branch, because **LR** states are stable only at higher concentrations $N > N_{hb}$ Bottom: The biaxiality parameter ([21]), $b = \sqrt{1 - \frac{6\,Tr(\mathbf{Q}^3)^2}{Tr(\mathbf{Q}^2)^3}}$, is depicted for each stable steady branch of Figure 2. This "degree of biaxiality" complements the birefringence projections (a) to assess whether the mesoscopic orientation $\mathbf{Q}(f)$ is close to uniaxial $(b = 0)$ or maximally biaxial $(b = 1)$.

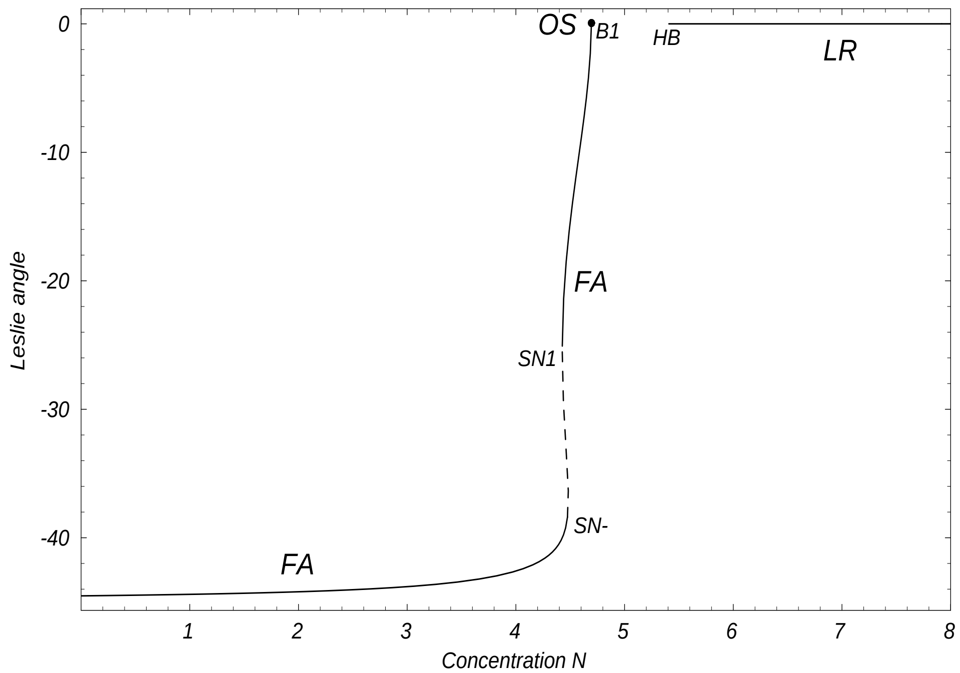

Figure 5: The Leslie in-plane, flow-alignment angle for steady stable solutions versus nematic concentration N at $Pe = 0.1$. The angle for the unstable steady flow-aligning solution is also shown.

Figure 3, incorrectly predicts bi-stable tumbling and logrolling stationary states for N between B_1 and HB (both are unstable), misses the kayaking attractor $\mathbf{K}_1$ altogether, misses the $\mathbf{K}_1$-**LR** transition at HB.

The Doi and Rey-Tsuji closures both capture the feature of instability of all in-plane (and **LR**) orientational distributions in weak shear inside a band of intermediate concentrations [9], though further details are sensitive to other model parameters.

Since no stable in-plane distributions exist, which out-of-plane orientational distributions emerge as the attracting states at this confluence of bifurcations around B_1?

- Figure 2c is the projection of each solution branch onto the *out-of-plane* component, $Re(a_{2,1})$, which is proportional to the second-moment tensor component, Q_{xz}. There is a nearly vertical, solid, black curve, with two distinguished points labelled $HB_{+,-}$, and a second red curve which persists from this critical concentration N_{SL_1} all the way to HB ($N = N_{hb}$) where the solution branch limits to the in-plane logrolling state. *Both of these solution branches are stable, out-of-plane modes*, but of quite different character.
  - The "apparently" vertical branch of Figure 2c is blown up in Figure 7, and corresponds to a *ring of out-of-plane, steady equilibria*, called **OS** by Faraoni et al.

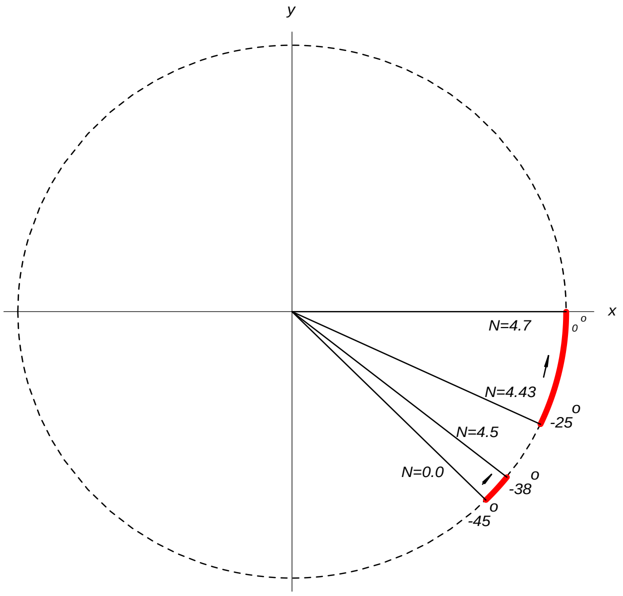

Figure 6: The change of the Leslie angle for steady flow-aligning solutions.

[6]. These branches occur so rapidly in N that the projection in Figure 2 appears vertical; stability terminates at bifurcations $HB_{+,-}$, Figure 7. The figures confirm the mirror-symmetry of the Smoluchowski equation (1); these states must occur in pairs. For $Pe = 0.1$ as illustrated, the **OS** states exist for an extremely narrow band of concentrations, approximately $4.695118 < N < 4.695193$.

– The role of these stable **OS** solution pairs appears to be that of accomplishing a "stiff steady transition" (versus N) from in-plane to out-of-plane alignment, which then undergoes an unsteady transition to kayaking motion! We amplify this mechanism in Figures 5-8.

First we plot the Leslie alignment angle for the in-plane **FA** branch in Figures 5 and 6; note convergence of the major director to the flow axis as one approaches the termination of the **FA** stable branch. This coincides with onset of the $\mathbf{OS}_{+,-}$ pair, which exists over an exceedingly short range of N. Figures 7,8 show the polar angle of the major director of the **OS** solution pair: the polar angle spans from the shearing plane at onset, all the way through approximately 72 degrees to within 18 degrees of the vorticity axis while $\Delta N \approx 10^{-4}$!

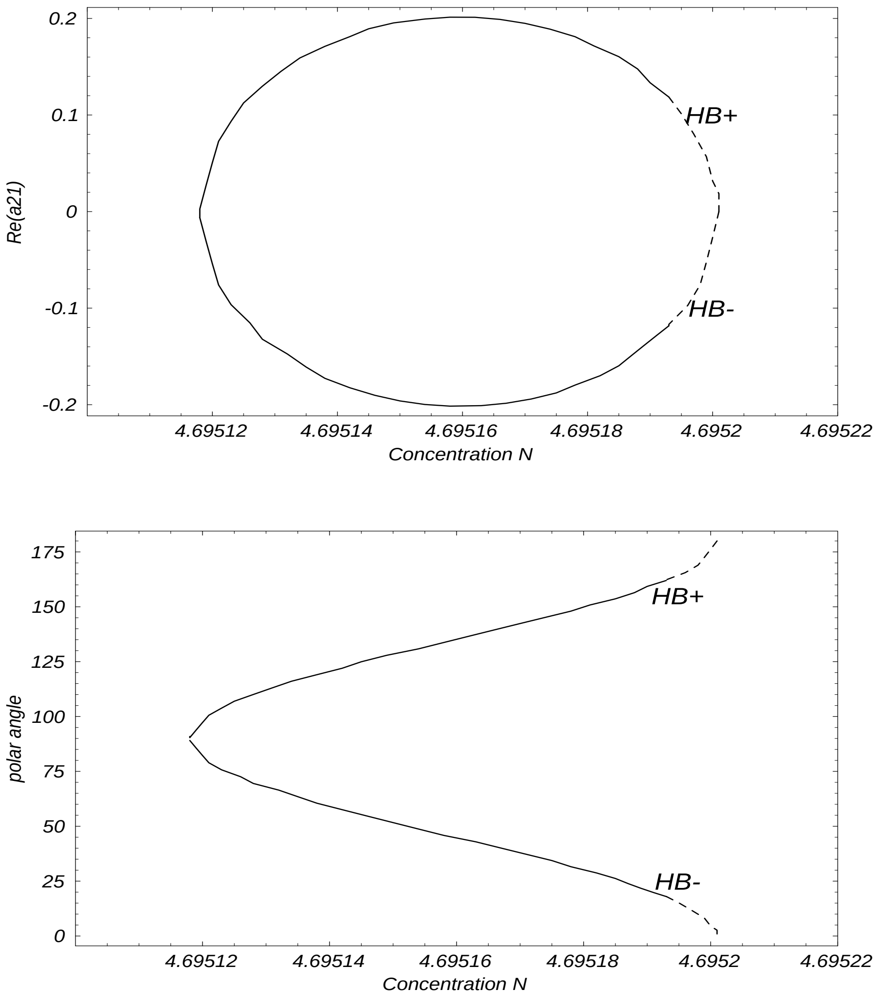

Figure 7: The out-of-plane steady solutions and their corresponding polar angle θ.

During this "stiff" transition in the polar angle, the Leslie angle remains nearly zero; the major director resides almost in the x-z plane (nearly completely orthogonal to the flow-gradient direction) for all **OS** states!

While these $\mathbf{OS}_{\pm}$ states are structurally unstable from the point of view of bifurcation theory [2], they play the role of transitioning from in-plane to out-of-plane stable alignment, followed by an instability of the **OS** states to kayaking motion. *To summarize*, the kinetic equation (1) does not yield a first-order phase transition from steady, in-plane **FA** to out-of-plane kayaking motion; *instead, kinetic theory predicts a continuous second-order* **FA** *to* $\mathbf{K}_1$ *transition, mediated by this stiff pair of stable* **OS** *states.* Several mesoscopic models capture these "rings" of *OS* pairs, including the Doi closure [9] and Landau-deGennes model [2].

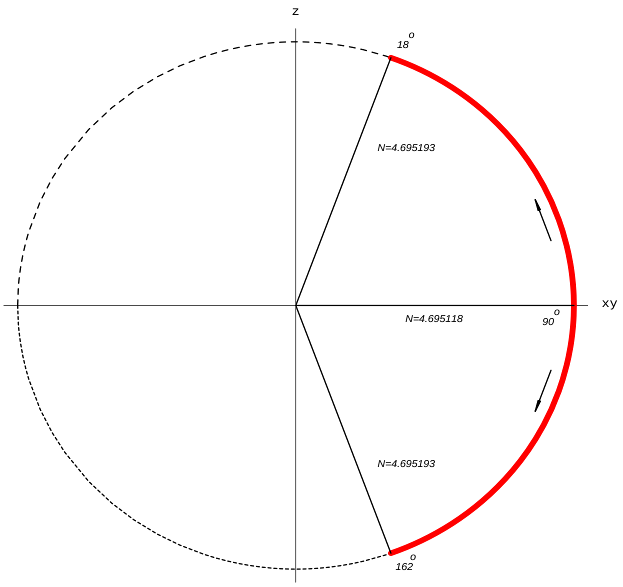

Figure 8: The polar angle θ of the out-of-plane stable steady solutions.

- At or very close to the termination of the **OS** branch pair, the unsteady transition to a stable "Larson-Ottinger" kayaking solution $\mathbf{K}_1$ occurs.

This is labelled SL_1 in Figure 2b; the analogous in-plane unsteady tumbling transition is labelled SL_2 in Figure 2b. Both this kayaking solution and the **OS** pair are absent in the in-plane Smoluchowski equation, Figure 3. The attractor that emerges is the single kayaking distribution function, whose mirror-symmetric orbit is itself. (We note that the projection onto the shearing plane of the major director $\mathbf{n}_1$ of $\mathbf{K}_1$ could be interpreted as a tumbling orbit experimentally).

- Therefore, the kayaking orbit $\mathbf{K}_1$ is the unique attractor for concentrations N between the bifurcations SL_1 and HB.

Detailed properties of the kayaking solution branch are given in Figures 9-14. Figure 9 depicts the period of $\mathbf{K}_1$ solutions for $N \in (N_{sl_1}, N_{hb})$. The birth at SL_1 of the $\mathbf{K}_1$ branch appears to coincide with an infinite-period Hopf bifurcation which we surmise emerges out of the **OS** "ring" of fixed points shown in Figure 7. However, we are unable to numerically resolve this structure, and guidance from bifurcation theory will be necessary (e.g., recent

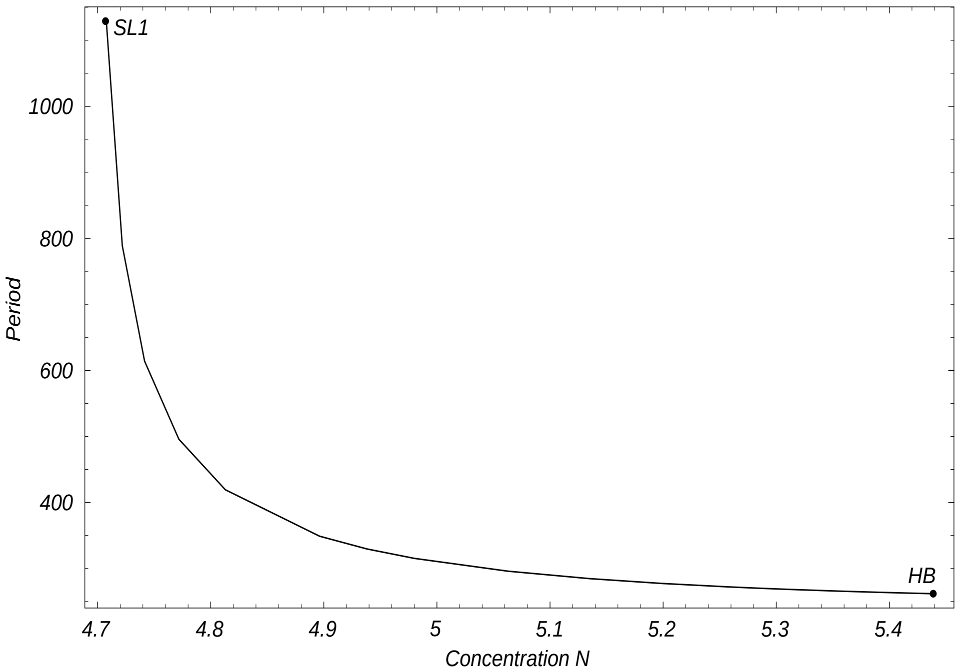

Figure 9: Periods for the kayaking solutions $\mathbf{K}_1$ for $Pe = 0.1$, between the bifurcation SL_1 and HB of Figure 2. Note the $\mathbf{K}_1 - \mathbf{LR}$ transition, which coincides with the termination of the kayaking branch, occurs at finite non-zero period (a Hopf bifurcation).

work of Chillingworth et al. [2] identifies the tumbling-wagging transition in terms of a Takens-Bogdanov bifurcation that extends the previous understanding from Farhoudi and Rey [5]). Figure 9 further shows the rapid decrease in period of the $\mathbf{K}_1$ branch to a finite period at HB where the $\mathbf{K}_1$-$\mathbf{LR}$ transition occurs through a Hopf bifurcation.

Figure 10 is a glimpse at slightly higher $Pe = 0.6$ where we are able to track the $\mathbf{K}_1$ branch which now overlaps for a narrow concentration band with the $\mathbf{OS}_\pm$ stable pair. $HB_\pm$ are infinite-period Hopf bifurcations as indicated by the software AUTO. We suspect there is some organizing structure that connects $HB_\pm$ with $\mathbf{K}_1$. The $\mathbf{K}_1$ genesis from Doi kinetic theory is not captured thus far by mesoscopic closure models [9].

Figure 11 illustrates the amplitudes of oscillation of the major director as computed for each kayaking distribution $f(\mathbf{m}, t)$. This is calculated by projection onto $\mathbf{Q}(f(\mathbf{m}, t))$, followed by determination of the largest eigenvalue d_1 of $\mathbf{M} = \mathbf{Q} + \frac{1}{3}\mathbf{I}$, whose eigenvector $\mathbf{n}_1$ is the major director. We then extract the maximum and minimum polar angle (with the vorticity axis) of $\mathbf{n}_1(f(\mathbf{m}, t))$ over the kayaking period. The graphs clearly show a convergence as N increases from N_{sl_1} to N_{hb}, beginning with large excursions away from the vorticity axis which close down onto the steady vorticity alignment of the $\mathbf{LR}$ branch.

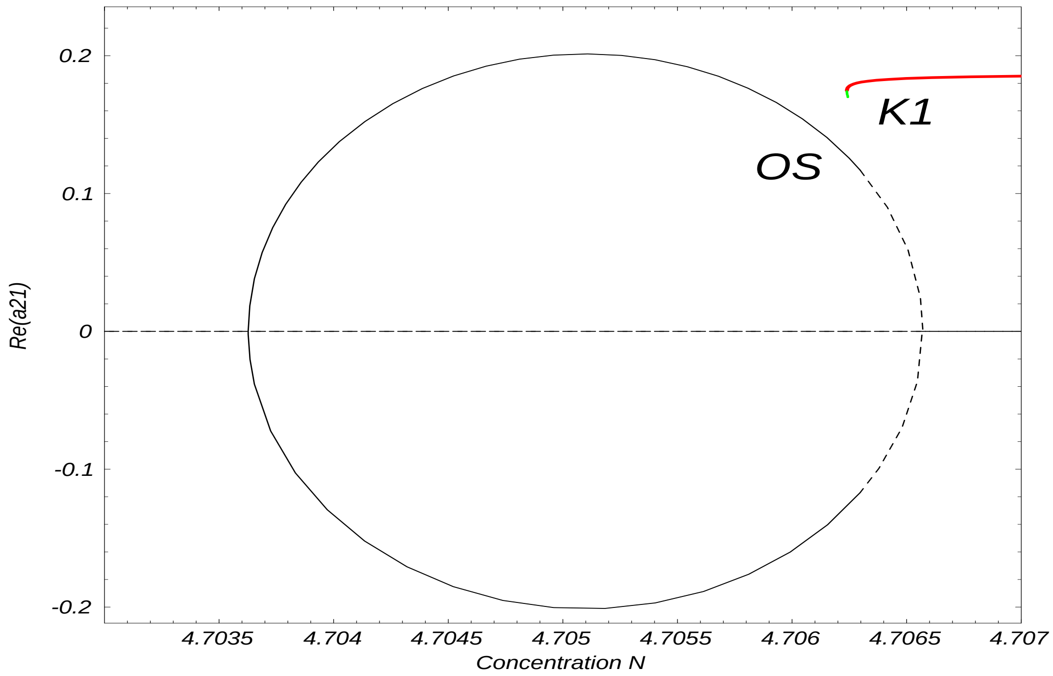

Figure 10: Co-existence of the stable, steady out-of-plane ($\mathbf{OS}^{+,-}$) pair of solutions (solid line) and the stable kayaking ($\mathbf{K}_1$) solution (grey line) for $Pe = 0.6$. In a very narrow region of (N, Pe), shown in Figure 15a and Table 1, these states yield tri-stability.

Figure 12 shows the maximum degree of orientation, d_1, is nearly constant for each kayaking orbit $\mathbf{K}_1$. This behavior suggests a "director-dominated" orientational dynamics of the attracting distributions $\mathbf{K}_1$. Figure 13 illustrates details of the particular $\mathbf{K}_1$ attractor at $N = 5.2$ and $Pe = 0.1$. The path of the "peak direction of the distribution $f(\mathbf{m}, t)$", as indicated by the major director $\mathbf{n}_1(f(\mathbf{m}, t))$, shows the classical Eskimo paddle oscillation imagined by Larson and Ottinger. Note the large polar angle excursions yet with the major director staying close to the x-z plane. I.e., the paddle stays at a shallow depth and never penetrates deep into the flow gradient direction. Figure 13b shows nearly constant birefringence in all planar cross-sections. Since $\mathbf{n}_1$ oscillates about the vorticity axis, $d_1 - d_3$ is the *maximum birefringence*, which is *greater than the* corresponding *quiescent maximum bifringence* $d_1 - d_2 = d_1 - d_3 = 0.654$ for $N = 5.2$. Note also that $d_2 - d_3 \approx 10^{-3}$, implying nearly uniaxial distributions $f(\mathbf{m}, t)$ throughout the orbit at this low shear rate.

Figure 14 illustrates two snapshots of the distribution function $f(\mathbf{m}, t)$ at the "apocenter" and "pericenter" of the $\mathbf{K}_1$ orbit for $N = 5.2, Pe = 0.1$. The vorticity-aligned quiescent nematic pdf for $N = 5.2, Pe = 0.0$ (Figure c) and the steady vorticity-aligned $\mathbf{LR}$ attractor for $N = 5.45, Pe = 0.1$ (Figure d) are shown for comparison.

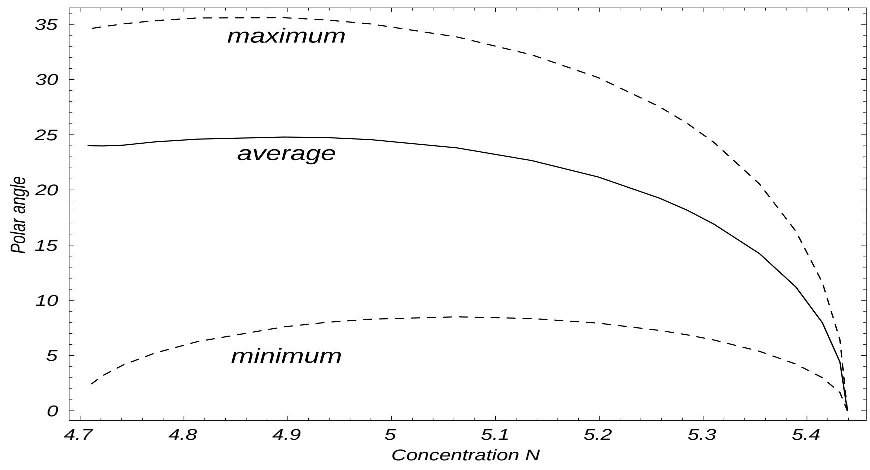

Figure 11: Maximum and minimum of the polar angle (from the vorticity axis) of the major director of $\mathbf{Q}(f)$ for the stable kayaking branch $\mathbf{K}_1$ (SL_1-HB, Figure 2), for $Pe = 0.1$. The branch terminates at HB in a $\mathbf{LR}$ transition through a finite-period Hopf bifurcation. This figure together with Figure 9, viewed from decreasing N, shows the $\mathbf{LR} - \mathbf{K}_1$ transition is a classical soft generation of limit cycles (the kayaking orbits), i.e., a second-order phase transition.

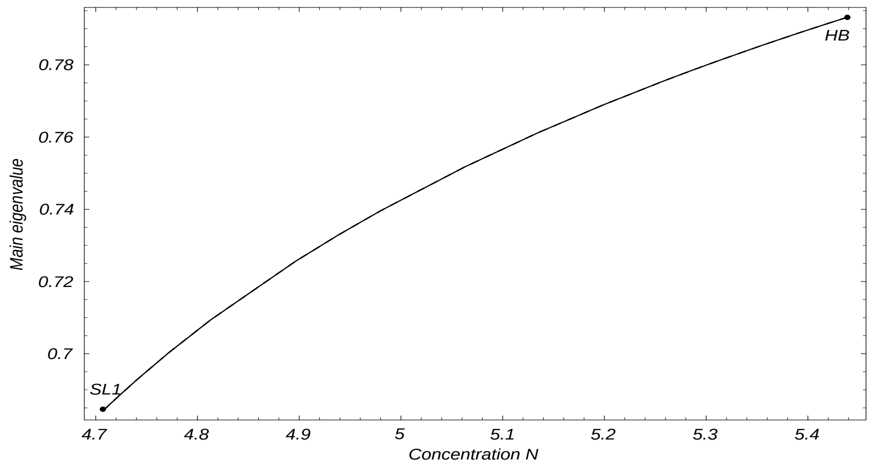

Figure 12: Maximum eigenvalue d_1 of the second-moment $\mathbf{M}(f)$ for the kayaking branch ($\mathbf{K}_1$) of solutions (SL_1-HB), Figure 2, $Pe = 0.1$. Each fixed attractor has nearly constant maximum degree of orientation with respect to the major director $\mathbf{n}_1$ of the distribution f. The relative maximum and minimum of $d_1(\mathbf{M}(f))$ over each kayaking orbit differ by less than 0.1 percent: the $\mathbf{K}_1$ orbits are "director-dominated". Note d_1 increases with N until the $\mathbf{LR}$ transition at HB when the director locks onto the vorticity axis, after which d_1 continues to increase with N as indicated in Figure 4a.

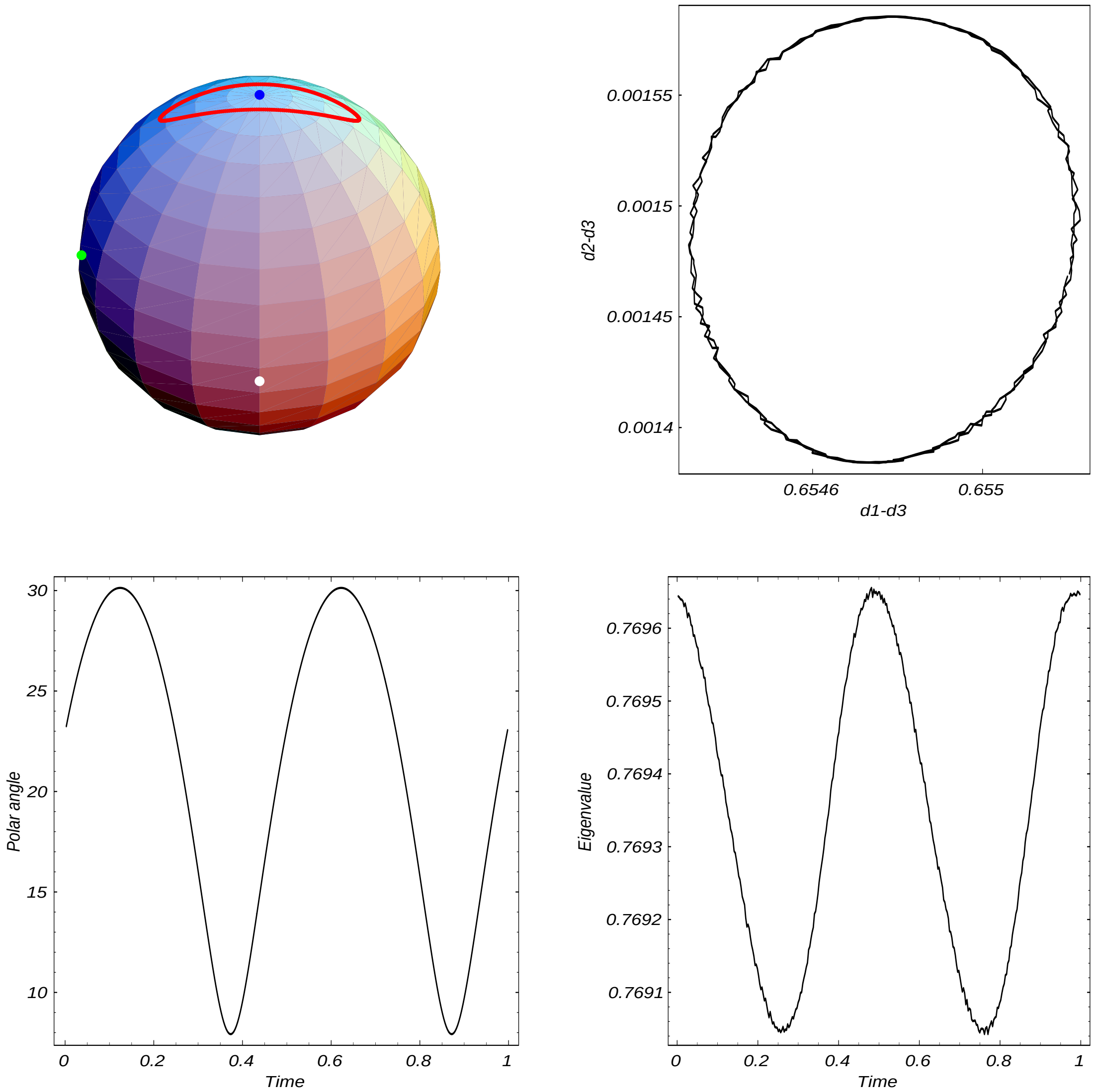

Figure 13: The Eskimo kayaking solution of Larson & Ottinger corresponding to the $N = 5.2$ orbit of Figures 11 and 12. The upper left picture shows the path of the major director on the unit sphere, calculated from $\mathbf{Q}(f(\mathbf{m}, t))$. The black dot shows the vorticity (z) axis, the grey dot shows the flow (x) direction, and the white dot marks the flow-gradient (y) direction. The order parameter statistics show two features: $d_2 - d_3 \approx 10^{-3}$, which indicates a weakly biaxial second-moment $\mathbf{Q}$ over the entire orbit; and $d_1 - d_3 \approx 0.65$ for all time indicating very little oscillation in the degrees of orientation. The $\mathbf{K}_1$ solutions are "director-dominated" orbits of the pdf f.

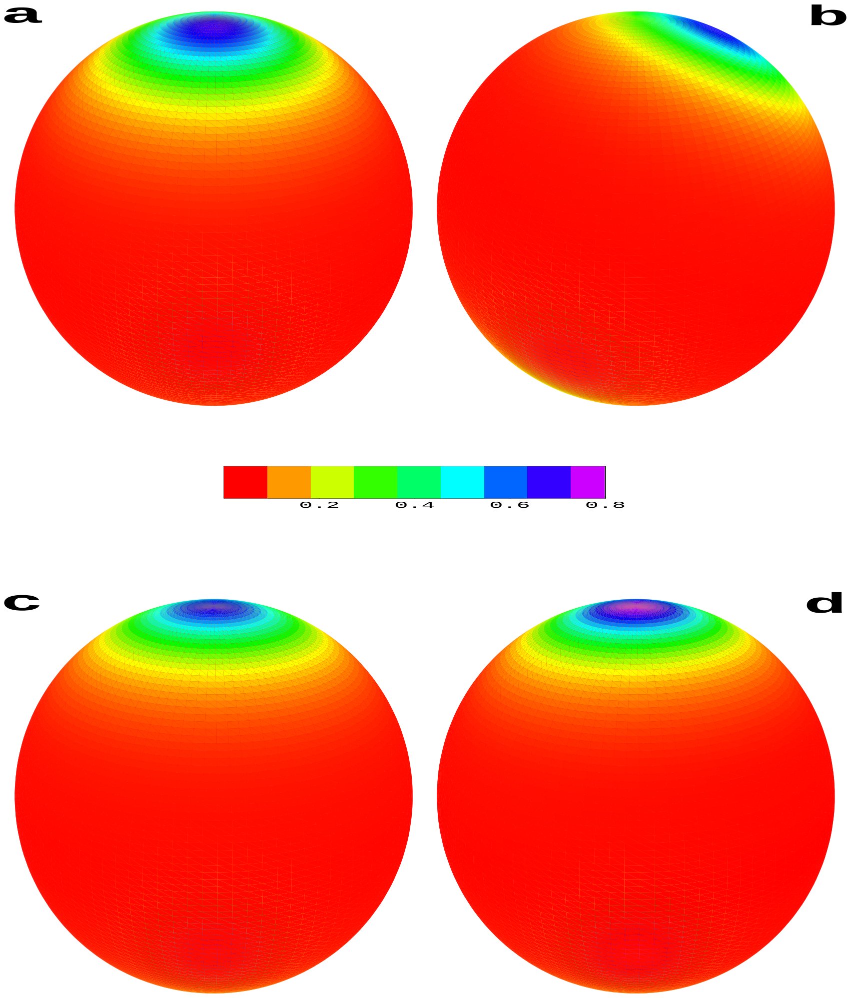

Figure 14: Figure c recalls [10] the *quiescent* nematic orientational distribution $f(\mathbf{m})$ of Figure 1 at $N = 5.2$, where $\mathbf{U} \in O(3)$ is chosen so that the distribution is peaked along the vorticity axis. Two snapshots (Figure a, b) depict $f(\mathbf{m}, t)$ along the stable kayaking orbit shown in Figure 13 for $N = 5.2$ and weak shear rate $Pe = 0.1$. The left (right) corresponds to the "pericenter" ("apocenter") where the most probable direction of orientation achieves minimum (maximum) distance to the vorticity axis. Figure d is the stable, steady **LR** distribution that emerges at $Pe = 0.1$ at slightly higher concentration (just past the Hopf bifurcation of Figure 15), $N = 5.45$, which illustrates enhanced focusing of the distribution along the vorticity axis. The color-intensity of these figures conveys shear-induced enhancement in the maximum degree of alignment, $d_1 = 0.7693$ for $Pe = 0, N = 5.2$, Figure c; $d_1 = 0.7693, 0.7696$ for $Pe = 0.1, N = 5.2$, Figure a, b; $d_1 = 0.7945$ for $Pe = 0.1, N = 5.45$, Figure d.

5 Continuation of the shear-selection mechanisms to finite shear rates, $0 < Pe < 1$

Finally, we are in position to summarize the multiplicity, stability, and steady versus unsteady properties of all stationary distributions of the Smoluchowski equation (1) for weak shear. The above figures and discussion give details for $Pe = 0.1$ and variable N, which we now continue for one more order of magnitude, $0.1 \leq Pe \leq 1$, in Figure 15 and Figure 16. These figures constitute the *weak shear, flow-phase diagram of nematic polymers*, indicating *eight distinct regions* in (N, Pe) where a fixed, finite set of stable solutions exist. We label these Regions I-VIII; Table 1 summarizes the attractor types and total multiplicity for each region.

- Regions I (low concentrations), II (intermediate concentrations), and III (high concentrations) consume the majority of the parameter space $0 \leq N \leq 8, 0.1 \leq Pe \leq 1$. Each has a unique attractor: in-plane steady **FA** states in Region I; out-of-plane periodic $\mathbf{K}_1$ states in Region II; and steady **LR** states in Region III.
- The small "fin" region IV for low Pe has *bi-stable* **FA** steady states. This is the weak-shear continuation of the quiescent concentration band $N_{sn} < N < N_{tc}$, Figure 1, where the isotropic (s_0) and nematic (s_+) steady states are bi-stable. The steady structure of Region IV inside of Region I also occurs in steady extensional flow [7, 8].
- Region V has *bi-stable, out-of-plane, steady states* labelled $OS^{+,-}$. These states have been described in Figures 6,7,8, and 10. Region V is the thin transition region between Region I and II, blown-up in Figures 15b and 16a.
- Region VI is an even thinner region between V and II where stable kayaking $\mathbf{K}_1$ and bi-stable $\mathbf{OS}^{+,-}$ states co-exist, shown in Figure 16a.
- Regions VII and VIII contain bi-stable "tilted kayaking" orbits ($\mathbf{K}_2^{+,-}$), respectively wagging ($\mathbf{W}$) attractors, which co-exist with the stable kayaking branch $\mathbf{K}_1$. These regions are only resolvable numerically for $Pe \geq 0.5$, Figure 15b, and blown up in Figure 16b.

The boundaries between these Regions of fixed attractors are summarized in Table 2. These correspond *physically* to various phase transitions, *mathematically* to specific bifurcation structures.

Table 2 provides some insights into the transition phenomena and corresponding states that are reponsible for the bifurcations between Regions. A few of these structures are straightforward "textbook" bifurcations:

- the saddle-nodes bounding regions IV and I

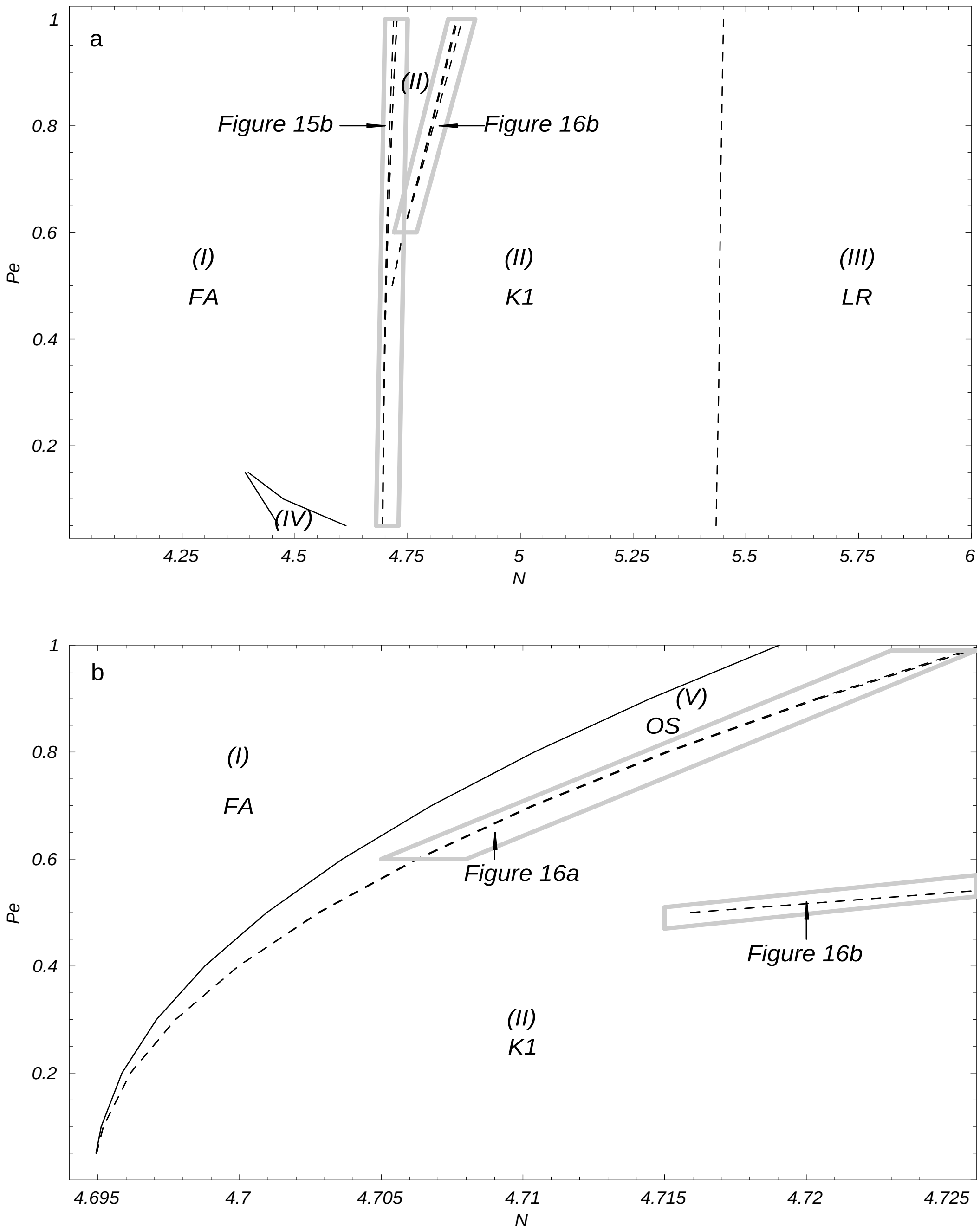

Figure 15: The concentration-flow (N, Pe) phase diagram of all stable orientational distributions and their transition boundaries. The top figure shows Regions I, II, III, and IV comprise the bulk of the diagram. More detailed structure unresolvable on the scale of the top figure is placed in grey frames and blown-up in the lower figure, and then blown-up again in Figure 16 to resolve further structure. The regions I and III persists for $0 < N < 4$ and $6 < N < 8$, respectively.

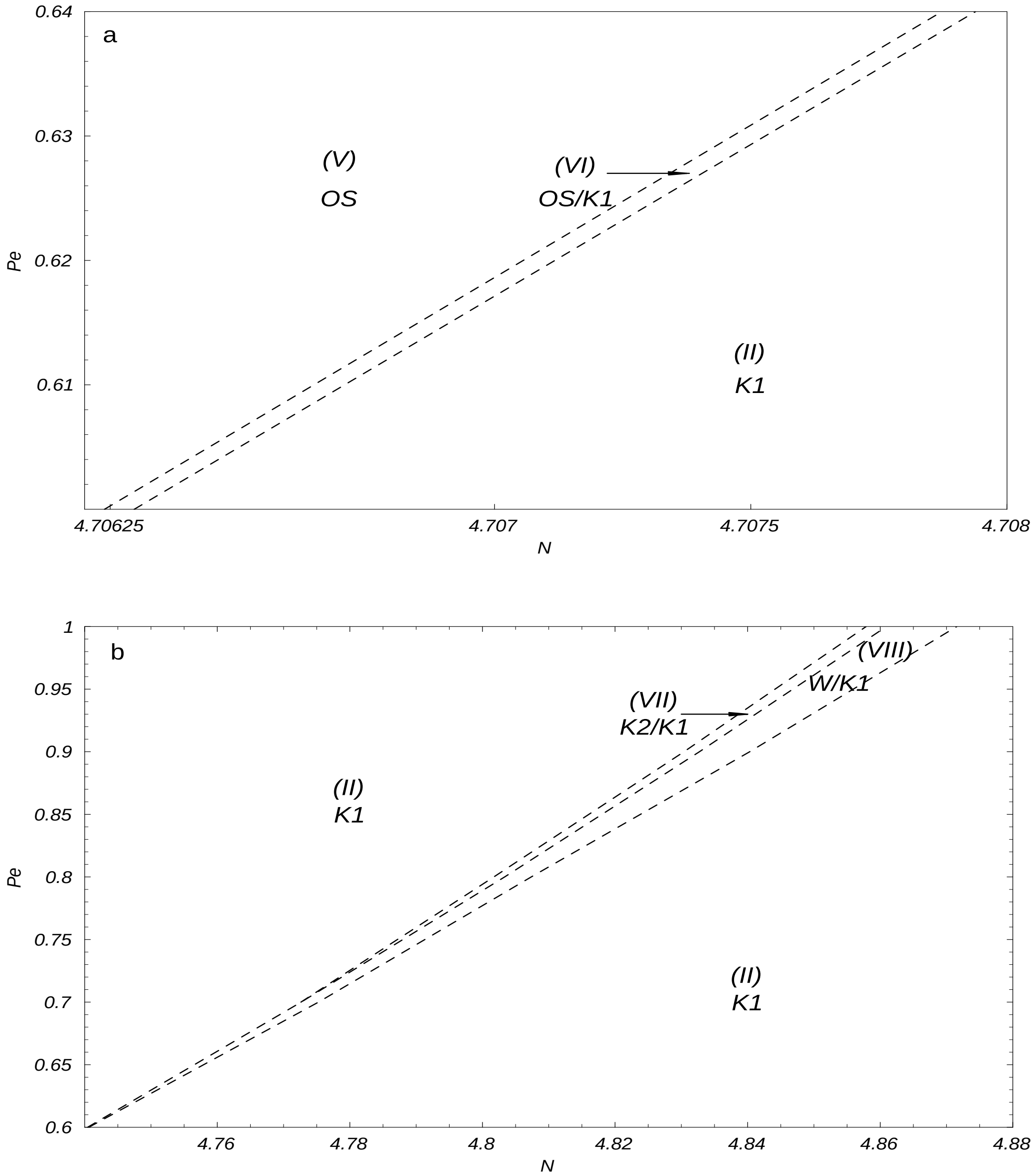

Figure 16: Blow-up of transition regions and boundaries from Figure 15. The top figure shows a sliver of parameter space in the transition between Regions V and II where the stable out-of-plane steady pair $\mathbf{OS}^{+,-}$ and the kayaking state $\mathbf{K}_1$ co-exist. Note the vertical scale is between $Pe = 0.6$ and $Pe = 0.64$, and the scale in N is even finer. The detailed structure from the top of Figure 15 with the small sliver that exists inside of Region II is blown up at the bottom. This marks the emergence at weak shear of Region VII where the wagging $\mathbf{W}$ state emerges, and Region VIII where stable pairs of "tilted kayaking" or "out-of-plane wagging" states $\mathbf{K}_2^{+,-}$ emerge. The boundary between these regions is the $\mathbf{W} - \mathbf{K}_2$ transition in which the in-plane periodic wagging mode undergoes an out-of-plane tipping instability, creating the pair of mirror-symmetric, out-of-plane tilted kayaking orbits.

Region	Attractor type	Attractor multiplicity
I	$\mathbf{FA}$	1
II	$\mathbf{K}_1$	1
III	$\mathbf{LR}$	1
IV	$\mathbf{FA}_1$, $\mathbf{FA}_2$	2
V	$\mathbf{OS}^+$, $\mathbf{OS}^-$	2
VI	$\mathbf{OS}^+$, $\mathbf{OS}^-$, $\mathbf{K}_1$	3
VII	$\mathbf{K}_1$, $\mathbf{K}_2^+$, $\mathbf{K}_2^-$	3
VIII	$\mathbf{W}$, $\mathbf{K}_1$	2

Table 1: Regions in (N, Pe) with type and number of pdf attractors. The Regions are defined in Figures 16 and 17.

- the $\mathbf{K}_1$-$\mathbf{LR}$ transition between II and III is a finite-period Hopf bifurcation
- the steady, in-plane to out-of-plane transition from $\mathbf{FA}$ to $\mathbf{OS}^{+,-}$ between regions I and V is a classical pitchfork bifurcation.

Yet other bifurcations are natural to large-dimensional dynamical systems. In Figure 17 we fix $N = 4.85$ and blow-up the vertical slice of Figure 16b for $0.9 \leq Pe \leq 1.0$ to amplify three more of the bifurcation boundaries at concentrations labelled $Pe_{1,2,3}$, all of which occur in the presence of the kayaking attractor $\mathbf{K}_1$:

- Pe_1: the unstable $\mathbf{T}$ (tumbling) to stable $\mathbf{W}$ (wagging) transition between regions II and VIII coincides with the emergence of an unstable $\mathbf{K}_2^{+,-}$ pair, which constitutes a pitchfork bifurcation of periodic solution branches.
- Pe_2: another periodic pitchfork bifurcation defines the transition regions VIII and VII where the stable $\mathbf{W}$ branch forks into an unstable $\mathbf{W}$ and a pair of stable $\mathbf{K}_2^{+,-}$ orbits.
- Pe_3: the first of a cascade of period-doubling bifurcations of the $\mathbf{K}_2^{+,-}$ attractors, which require further blow-up. This region marks entrance into the chaotic regime discovered by Grosso et al. [14], the details of which are beyond this paper. Remarkably, this period-doubling route to chaotic dynamics is captured by the Doi closure with finite aspect-ratio molecules [9].

The bifurcation between regions V and VI requires further clarification both theoretically and numerically.

Boundary (left to right)	Bifurcation type	Attractor transition (left to right regions)
I-II	saddle node	unique to bi-stable **FA**
II-I	saddle node	bi-stable to unique **FA**
I-V	steady pitchfork	steady in-plane **FA** to out-of-plane $\mathbf{OS}^{+,-}$ transition
V-VI	saddle-loop	onset of $\mathbf{K}_1$ attractor
VI-II	∞-period, unstable Hopf	stable to unstable transition of $\mathbf{OS}^{+,-}$
II-VII	complex period-doubling cascade (requires further blow-up)	emergence of out-of-plane, periodic, bi-stable $\mathbf{K}_2^{+,-}$
VII-VIII	periodic pitchfork	unstable to stable transition of **W** and stable to unstable transition of $\mathbf{K}_2^{+,-}$
VIII-II	periodic pitchfork	stable **W** to unstable **T** transition and loss of unstable $\mathbf{K}_2^{+,-}$ pair
II-III	supercritical, finite-period Hopf	periodic $\mathbf{K}_1$ to steady **LR** transition

Table 2: Attractor transitions for nematic polymers in weak shear $0 < Pe \leq 1$, and for the dilute to concentrated range $0 < N < 8$. The regions are defined in Figure 15, 16 and the fixed attractors in each region are listed in Table 1.

6 Conclusion

The weak-shear monodomain attractors and transition phenomena have been detailed here, and are now poised to guide the continuation into higher shear rates. A variety of subtle attractor properties of the Doi kinetic theory have been clarified by a combination of mesoscopic predictions and detailed kinetic theory simulations. The issue of multiplicity, in-plane versus out-of-plane, and stability of stationary orientational distributions have been mostly resolved in this study, and the remaining questions have been identified.

These detailed kinetic attractor regimes also serve as benchmarks for closure approximations. Clearly, the bifurcation phenomena amplified here will defy any attempt to capture the entire structure with second-moment closures, as we have annotated during the discussions. Specific closures are capable of reproducing quite complex features *if* one restricts to

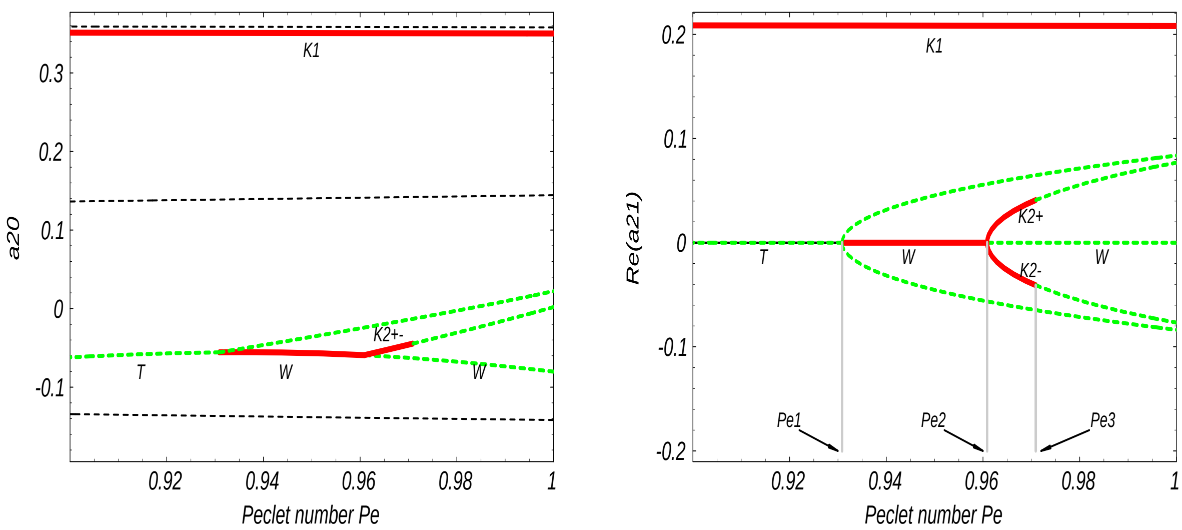

Figure 17: A vertical slice of Figure 16b for fixed concentration $N = 4.85$ and variable $0.9 < Pe < 1$. The stable $\mathbf{K}_1$ branch exists independently of the three bifurcations labelled $Pe_{1,2,3}$. The unstable $\mathbf{T}$ to stable $\mathbf{W}$ transition coincides with onset of an unstable, out-of-plane kayaking pair $\mathbf{K}_2^{+,-}$, which together comprise a periodic pitchfork bifurcation (ppb). Another ppb occurs at Pe_2, where the $\mathbf{W}$ branch becomes unstable, sparing a stable pair of $\mathbf{K}_2^{+,-}$. Finally, at Pe_3, both $\mathbf{K}_2^+$ and $\mathbf{K}_2^-$ undergo ppb creating *four* stable $\mathbf{K}_2$ branches. This marks the onset of a rapid sequence of period-doubling bifurcations discovered by Grosso et al. [14].

a limited region of (N, Pe) space. With respect to the rich bifurcation structures in weak shear, there do not appear to be any *a priori* closure rules capable of capturing the flow-phase diagram of kinetic theory.

References

[1] Burghardt, W.R., Macromol. Chem. Phys. **199**, 471-488 (1998).

[2] Chillingworth, D.R.J., Alonso, E.V., Wheeler, A.A., J. Phys. A: Math. Gen. **34**, 1393-1404 (2001).

[3] deGennes, P-G, Prost, J., **The Physics of Liquid Crystals**, Oxford University Press (1993).

[4] Doi, M., J. Polym. Sci., Polym. Phys. Ed. **19**, 229 (1981).

[5] Farhoudi, Y., Rey, A.D., J. Rheol. **37**, 289-314 (1993).

[6] Faraoni, V., Grosso, M., Crescitelli, S., Maffettone, P. L., J. Rheol. **43**, 829 (1999).

[7] Forest, M.G., Wang, Q., Zhou, H. Physics Fluids, **12**(3), 490-498 (2000)

[8] Forest, M.G., Wang, Q., Zhou, H. Liquid Crystals, **28**(5), 717-720, 2001

[9] Forest, M.G., Wang, Q., Rheol. Acta, to appear (2002).

[10] Forest, M.G., Wang, Q., Zhou, R., Symmetries of the Doi kinetic theory for nematic polymers of arbitrary aspect ratio: at rest and in linear flows, UNC Program in Applied Mathematics Preprint No. PAMPS-2002-08 (2002), submitted to Physical Review E.

[11] Forest, M.G., Wang, Q., Zhou, R., Full tensor alignment criteria for nematic polymers in weak shear. UNC Program in Applied Mathematics Preprint No. PAMPS-2002-17 (2002),

[12] Fuller, G.G., **Optical Rheometry of Complex Fluids**, Oxford University Press, Oxford (1995).

[13] Gear, C.W., Kevrekidis, I.G., Preprint, Princeton University, (2001).

[14] Grosso, M., Keunings, R., Crescitelli, S., Maffettone, P.L., Prediction of chaotic dynamics in sheared liquid crystalline polymers, Preprint (2001) and lecture, Society of Rheology Annual Meeting, Hilton Head, SC, February (2001).

[15] Hess, S., Z. Naturforsch Teil **31A**, 1034 (1976).

[16] Hinch, E.J., Leal, L.G., J. Fluid Mech. **76**(1), 187 (1976).

[17] Kuzuu, N., Doi, M.J., Phys. Soc. Japan **52**, 3486 (1983).

[18] Kuzuu, N., Doi, M. J., Phys. Soc. Japan **53**, 1031 (1984).

[19] Larson, R.G., Macromolecules **23**, 3983 (1990).

[20] Larson, R.G., Ottinger, H., Macromolecules **24**, 6270 (1991).

[21] Maffettone, P.L., Sonnet, A.M., Virga, E.G., J. Non-Newt. Fluid Mech. **90**, 283-297 (2000).

[22] Marrucci, G., Macromolecules **24**, 4176-4182 (1991).

[23] Marrucci, G., Greco, F., Mol. Cryst. Liq. Cryst. **206**, 17 (1991).

[24] Marrucci, G., Greco, F., Adv. Chem. Phys. **86**, 331 (1993).

[25] Marrucci, G., Maffetone, P.L., Macromolecules **22**, 4076-4082 (1989).

[26] Messiah, Albert, **Quantum Mechanics.** Volume 2, North-Holland Publishing Company, Amsterdam, 1964

[27] Rienacker, G., Hess, S., Phyica A **267**, 294-321 (1999).

[28] Semenov, A.N., Sov. Phys. J.E.T.P. **85**, 321 (1983).

[29] Semenov, A.N., Sov. Phys. J.E.T.P. **66**, 712 (1986).

[30] Theodoropoulos, C., Qian, Y., Kevrekidis, I.G., Proceedings of the National Academy of Sciences. **97**, 2000.

[31] Tsuji, T., Rey, A.D., J Non-Newtonian Fluid Mech. **73**, 127 (1997).

[32] Wang, Q., A hydrodynamic theory for solutions of nonhomogeneous nematic liquid crystalline polymers of different configuration, J. Chem Phys., to appear (2002).